

ARMY RESEARCH LABORATORY



A Two-Dimensional Meteorological Computer Model for the Forest Canopy

by Arnold Tunick

ARL-MR-569

August 2003

NOTICES

Disclaimers

The findings in this report are not to be construed as an official Department of the Army position, unless so designated by other authorized documents.

Citation of manufacturers' or trade names does not constitute an official endorsement or approval of the use thereof.

Army Research Laboratory

Adelphi, MD 20783-1197

ARL-MR-569**August 2003**

A Two-Dimensional Meteorological Computer Model for the Forest Canopy

Arnold Tunick

Computational and Information Sciences Directorate, ARL

REPORT DOCUMENTATION PAGE			Form Approved OMB No. 0704-0188		
Public reporting burden for this collection of information is estimated to average 1 hour per response, including the time for reviewing instructions, searching existing data sources, gathering and maintaining the data needed, and completing and reviewing the collection information. Send comments regarding this burden estimate or any other aspect of this collection of information, including suggestions for reducing the burden, to Department of Defense, Washington Headquarters Services, Directorate for Information Operations and Reports (0704-0188), 1215 Jefferson Davis Highway, Suite 1204, Arlington, VA 22202-4302. Respondents should be aware that notwithstanding any other provision of law, no person shall be subject to any penalty for failing to comply with a collection of information if it does not display a currently valid OMB control number. PLEASE DO NOT RETURN YOUR FORM TO THE ABOVE ADDRESS.					
1. REPORT DATE (DD-MM-YYYY) August 2003		2. REPORT TYPE Final		3. DATES COVERED (From - To) October 2002–June 2003	
4. TITLE AND SUBTITLE A Two-Dimensional Meteorological Computer Model for the Forest Canopy			5a. CONTRACT NUMBER		
			5b. GRANT NUMBER		
			5c. PROGRAM ELEMENT NUMBER 61102A		
6. AUTHOR(S) Arnold Tunick			5d. PROJECT NUMBER 3FEJ00		
			5e. TASK NUMBER		
			5f. WORK UNIT NUMBER		
7. PERFORMING ORGANIZATION NAME(S) AND ADDRESS(ES) U.S. Army Research Laboratory Attn: AMSRL-CI-EE 2800 Powder Mill Road Adelphi, MD 20783-1197			8. PERFORMING ORGANIZATION REPORT NUMBER ARL-MR-569		
9. SPONSORING/MONITORING AGENCY NAME(S) AND ADDRESS(ES) U.S. Army Research Laboratory 2800 Powder Mill Road Adelphi, MD 20783-1197			10. SPONSOR/MONITOR'S ACRONYM(S)		
			11. SPONSOR/MONITOR'S REPORT NUMBER(S)		
12. DISTRIBUTION/AVAILABILITY STATEMENT Approved for public release; distribution unlimited.					
13. SUPPLEMENTARY NOTES AMS Code: 6110253A11 DA Project: B53A					
14. ABSTRACT This report presents the equation set, modeling assumptions, and some initial results from a new, physics-based computer model that is being developed for two-dimensional forest canopy wind flow, temperature, and turbulence calculations. The model is based on the conservation (simplified Navier-Stokes) equations for continuity, momentum, Reynolds stress, energy, heat flux, and turbulent temperature variance. A set of simultaneous equations for each of 12 computed variables is solved iteratively on a computational grid consisting of 10 × 60 points. Horizontal grid spacing is 50 m, and vertical grid spacing is 0.5 m. The model domain is 500 × 30 m. It is anticipated that improved turbulence and micrometeorological models for forest canopies will become increasingly useful for military acoustic application research.					
15. SUBJECT TERMS Conservation equations, wind flow, energy budget, and computational methods					
16. SECURITY CLASSIFICATION OF:			17. LIMITATION OF ABSTRACT UL	18. NUMBER OF PAGES 30	19a. NAME OF RESPONSIBLE PERSON Arnold Tunick
a. REPORT UNCLASSIFIED	b. ABSTRACT UNCLASSIFIED	c. THIS PAGE UNCLASSIFIED			19b. TELEPHONE NUMBER (Include area code) (301) 394-1765

Contents

Contents	iii
List of Figures	iv
Acknowledgments	v
1. Introduction	1
2. Forest Canopy Model	1
2.1 Conservation Equations.....	1
2.2 Modeling Assumptions.....	3
2.3 Second-Order Turbulence Closure Model for 2-D Forest Canopies.....	5
2.4 Numerical Methods	8
2.5 Forest Canopy Architecture.....	10
3. Model Results	10
3.1 Uniform Forest Stands	10
3.2 Nonuniform Forest Stands.....	13
4. Summary and Conclusions	18
5. References	19

List of Figures

Figure 1. Normalized vertical profiles of leaf area density for forest canopies.....	10
Figure 2. Model results for uniform forest stands: (a) horizontal wind velocity, $\langle \bar{u} \rangle$, in units ms^{-1} , and (b) air temperature, $\langle \bar{\theta} \rangle$, in units $^{\circ}\text{C}$. For this example, canopy height (h) is 10 m	11
Figure 3. Profiles of horizontal wind velocity ($\langle \bar{u} \rangle$, in units ms^{-1}) and air temperature ($\langle \bar{\theta} \rangle$, in units $^{\circ}\text{C}$) derived from the current 2-D calculation shown in comparison to 1-D profiles derived from an earlier study	12
Figure 4. Spurious oscillations due to numerical instability in the 2-D model results for uniform forest stands. The computed variable is horizontal wind velocity, $\langle \bar{u} \rangle$, in units ms^{-1}	12
Figure 5. Model results for nonuniform forest stands, i.e., those that contain a single step change in canopy height: (a) horizontal wind velocity, $\langle \bar{u} \rangle$, in units ms^{-1} , and (b) wind flow streamlines. A single step change in canopy height at $X/2 + \Delta x$ is shown using open rectangles, where $h = 8$ m on the left side and $h = 10$ m on the right side	13
Figure 6. Model results for nonuniform forest stands: (a) vertical wind velocity, $\langle \bar{w} \rangle$, in units ms^{-1} and (b) kinematic (fluctuation) pressure $\langle \bar{p} \rangle$, in units $\text{m}^{-2}\text{s}^{-2}$. A single step change in canopy height occurs at $X/2 + \Delta x$, where $h = 8$ m on the left side and $h = 10$ m on the right side	14
Figure 7. Model results for nonuniform forest stands: (a) air temperature, $\langle \bar{\theta} \rangle$, in units $^{\circ}\text{C}$ and (b) effective speed of sound, $\langle \bar{C}_{\text{eff}} \rangle$, in units ms^{-1} . A single step change in canopy height occurs at $X/2 + \Delta x$, where $h = 8$ m on the left side and $h = 10$ m on the right side	14
Figure 8. Spurious oscillations due to numerical instability in the 2-D model results for nonuniform forest stands. The computed variable is horizontal wind velocity, $\langle \bar{u} \rangle$, in units ms^{-1}	15
Figure 9. Model results for nonuniform forest stands, i.e., those that contain a single step change in canopy height: (a) horizontal wind velocity, $\langle \bar{u} \rangle$, in units ms^{-1} , and (b) wind flow streamlines. A single step change in canopy height at $X/2 + \Delta x$ is shown using open rectangles, where $h = 4$ m on the left side and $h = 10$ m on the right side	16
Figure 10. Model results for nonuniform forest stands: (a) vertical wind velocity, $\langle \bar{w} \rangle$, in units ms^{-1} , and (b) kinematic (fluctuation) pressure $\langle \bar{p} \rangle$, in units $\text{m}^{-2}\text{s}^{-2}$. A single step change in canopy height occurs at $X/2 + \Delta x$, where $h = 4$ m on the left side and $h = 10$ m on the right side	16
Figure 11. Model results for nonuniform forest stands: (a) air temperature, $\langle \bar{\theta} \rangle$, in units $^{\circ}\text{C}$, and (b) effective speed of sound, $\langle \bar{C}_{\text{eff}} \rangle$, in units ms^{-1} . A single step change in canopy height occurs at $X/2 + \Delta x$, where $h = 4$ m on the left side and $h = 10$ m on the right side.....	17
Figure 12. Numerical instability, i.e., $2\Delta x$ waves, in the computation of wind flow streamlines for nonuniform forest stands: (a) $\int d\psi = -\int w dx + \int u dz$ and (b) $\int d\psi = -\int w dx$ only. A single step change in canopy height occurs at $X/2 + \Delta x$, where $h = 4$ m on the left side and $h = 10$ m on the right side.....	17

Acknowledgments

The author would like to thank Ronald Meyers, Keith Deacon, and Yansen Wang of the U.S. Army Research Laboratory for many helpful discussions on computational methods. The Department of the Army funded this research through Project B53A/61102A.

INTENTIONALLY LEFT BLANK.

1. Introduction

In a previous study (1, 2), it was found that a useful mathematical representation of the wind flow, temperatures, and turbulence inside and above a (uniform) continuous forest stand could be obtained by means of a one-dimensional (1-D), steady-state, second-order turbulence closure model, with an embedded radiative transfer and energy budget algorithm to predict the heat source. Development of this model made it possible to generate realistic profiles for effective sound speed inside and above a forest canopy. In turn, these data were used as input to an acoustic propagation model that predicts atmospheric and terrain effects on short-range acoustic attenuation (3, 4). As a result, it was shown that attenuation and “ducting” of acoustic waves in and around forests is significantly influenced by local micrometeorological profile structure.

However, forest stands are typically inhomogeneous, containing nonuniform distributions of canopy height and leaf area density (5). In addition, open fields, roadways, and buildings often border forests. Hence, to begin to address nonuniform forests and forest edges, this report presents the equation set, modeling assumptions, and some initial results from a new, physics-based computer model that is being developed for two-dimensional (2-D) forest canopy wind flow, temperature, and turbulence calculations. Like the earlier 1-D model, the 2-D model is based on the conservation (simplified Navier-Stokes) equations for continuity, momentum, Reynolds stress, energy, heat flux, and turbulent temperature variance. However, in this case, a set of simultaneous equations for each of 12 computed variables is solved iteratively on a computational grid consisting of 10×60 points. Horizontal grid spacing is 50 m and vertical grid spacing is 0.5 m. The model domain is 500×30 m. It is anticipated that improved physics-based theory and computer modeling for meteorology coupled to acoustics will become increasingly useful to predict effective sound speed information for military acoustic application research (6, 7).

The mathematical model for the forest canopy is described in section 2. Initial model results for uniform forest stands are shown in section 3.1. Initial model results for nonuniform forest stands, i.e., those that contain a single step change in canopy height, are shown in section 3.2. A summary and conclusions are provided in section 4.

2. Forest Canopy Model

2.1 Conservation Equations

The conservation (simplified Navier Stokes) equations for the current model, neglecting coriolis* forces, can be expressed as follows:

*Other than a few authors (8–10), most consider the effect of the coriolis force as being negligible for the scales of motion considered.

The continuity equation is

$$-\frac{1}{\langle \bar{\rho} \rangle} \frac{\partial \langle \bar{\rho} \rangle}{\partial t} = 0 = \frac{\partial \langle \bar{u}_i \rangle}{\partial x_i}. \quad (1)$$

The momentum equation is

$$\frac{\partial \langle \bar{u}_i \rangle}{\partial t} = 0 = - \left\langle \bar{u}_j \frac{\partial \bar{u}_i}{\partial x_j} \right\rangle - \frac{\partial \langle \bar{u}_i \bar{u}_j' \rangle}{\partial x_j} - \left(\left\langle \bar{u}_j \frac{\partial \bar{p}}{\partial x_i} \right\rangle + \left\langle \bar{u}_i \frac{\partial \bar{p}''}{\partial x_j} \right\rangle \right) + \frac{g \theta_0}{T} \delta_{i3} + \nu \left(\frac{\partial^2 \langle \bar{u}_i \rangle}{\partial x_j \partial x_j} + \left\langle \frac{\partial^2 \bar{u}''}{\partial x_j \partial x_j} \right\rangle \right). \quad (2)$$

Here, t is the independent variable time, $\bar{\rho}$ is air density, \bar{u}_i is the i -component of the wind velocity vector ($u_1 = \bar{u}$, $u_2 = \bar{v}$, $u_3 = \bar{w}$), and x_i is the i -component of the position vector ($x_1 = x$, $x_2 = y$, $x_3 = z$). In addition, p is static pressure normalized by air density (i.e., kinematic pressure), g is the acceleration due to gravity, T is the absolute temperature, θ_0 is a deviation from a reference temperature that decreases with height at the adiabatic lapse rate, and ν is kinematic viscosity. The overbar and primed variables indicate the mean (time averaged) and fluctuating components of the given quantity, whereas the brackets, $\langle \rangle$, and double primed variables indicate horizontal averaging and departures from the horizontal averaging operator (11).

The stress equation for non-adiabatic conditions is

$$\begin{aligned} \frac{\partial \langle \bar{u}_i \bar{u}_k' \rangle}{\partial t} = 0 = & - \langle \bar{u}_j \rangle \frac{\partial \langle \bar{u}_i \bar{u}_k' \rangle}{\partial x_j} - \left(\langle \bar{u}_j \bar{u}_k' \rangle \frac{\partial \langle \bar{u}_i \rangle}{\partial x_j} + \langle \bar{u}_i \bar{u}_j' \rangle \frac{\partial \langle \bar{u}_k \rangle}{\partial x_j} \right) - \left(\frac{\partial \langle \bar{u}_i \bar{u}_j \bar{u}_k' \rangle}{\partial x_j} \right) + \frac{g}{T} \left(\langle \bar{u}_i \bar{\theta}' \rangle \delta_{k3} + \langle \bar{u}_k \bar{\theta}' \rangle \delta_{i3} \right) \\ & - \left(\left\langle \bar{u}_k' \frac{\partial \bar{p}}{\partial x_i} \right\rangle + \left\langle \bar{u}_i' \frac{\partial \bar{p}}{\partial x_k} \right\rangle \right) + \left(\langle \bar{u}_k \rangle \left\langle \frac{\partial \bar{p}''}{\partial x_i} \right\rangle + \langle \bar{u}_i \rangle \left\langle \frac{\partial \bar{p}''}{\partial x_k} \right\rangle \right) + \nu \left(-2 \left\langle \frac{\partial \bar{u}_i \bar{u}_k'}{\partial x_j \partial x_j} \right\rangle + \frac{\partial^2 \langle \bar{u}_i \bar{u}_k'' \rangle}{\partial x_j \partial x_j} \right). \end{aligned} \quad (3)$$

The energy equation is

$$\frac{d \langle \bar{\theta} \rangle}{dt} = 0 = - \langle \bar{u}_k \rangle \frac{\partial \langle \bar{\theta} \rangle}{\partial x_k} - \frac{\partial \langle \bar{u}_k \bar{\theta}' \rangle}{\partial x_k} + \kappa_T \frac{\partial^2 \langle \bar{\theta} \rangle}{\partial x_k \partial x_k} + S_\theta. \quad (4)$$

Here, θ is ambient air temperature, κ_T is thermal diffusivity, and S_θ is the forest canopy heat source (or sink). The heat source can be expressed as a function of leaf surface-to-ambient-air temperature differences (12).

The heat flux equation is

$$\begin{aligned} \frac{\partial \langle \overline{u_j \theta'} \rangle}{\partial t} = 0 = & -\langle \overline{u_k} \rangle \frac{\partial \langle \overline{u_j \theta'} \rangle}{\partial x_k} - \langle \overline{u_j u_k} \rangle \frac{\partial \langle \overline{\theta} \rangle}{\partial x_k} - \langle \overline{\theta' u_k} \rangle \frac{\partial \langle \overline{u_j} \rangle}{\partial x_k} - \frac{\partial \langle \overline{u_j u_k \theta'} \rangle}{\partial x_k} + \frac{g}{T} \langle \overline{\theta'^2} \rangle \delta_{j3} \\ & + \left\langle \overline{p' \frac{\partial \theta'}{\partial x_j}} \right\rangle - (\kappa_T + \nu) \left\langle \overline{\frac{\partial u_j}{\partial x_k} \frac{\partial \theta'}{\partial x_k}} \right\rangle. \end{aligned} \quad (5)$$

Finally, the turbulent temperature variance equation is

$$\frac{\partial \langle \overline{\theta'^2} \rangle}{\partial t} = 0 = -\langle \overline{u_k} \rangle \frac{\partial \langle \overline{\theta'^2} \rangle}{\partial x_k} - 2 \langle \overline{u_k \theta'} \rangle \frac{\partial \langle \overline{\theta} \rangle}{\partial x_k} - \frac{\partial \langle \overline{u_k \theta'^2} \rangle}{\partial x_k} - 2\kappa_T \left\langle \overline{\frac{\partial \theta'}{\partial x_k} \frac{\partial \theta'}{\partial x_k}} \right\rangle. \quad (6)$$

2.2 Modeling Assumptions

Wilson and Shaw (13) give the following closure approximation for the pressure drag force in equation 2:

$$\frac{\partial \overline{p'}}{\partial x_i} = C_d A |\overline{U}| \langle \overline{u_i} \rangle. \quad (7)$$

Here, C_d is the forest canopy drag coefficient ($= 0.10$) and A (in units $\text{m}^2 \text{m}^{-3}$) is the leaf area density. It is further assumed that pressure forces are the main contributor to the total drag from the forest canopy (i.e., viscous drag forces are neglected).

In equation 3, Mellor (14) and Mellor and Yamada (15, 16) parameterize the triple-velocity products as

$$\langle \overline{u_i u_j u_k} \rangle = -q \lambda_1 \left[\frac{\partial \langle \overline{u_j u_k} \rangle}{\partial x_i} + \frac{\partial \langle \overline{u_i u_j} \rangle}{\partial x_k} + \frac{\partial \langle \overline{u_i u_k} \rangle}{\partial x_j} \right], \quad (8)$$

where the turbulent kinetic energy (t.k.e.) is $q = \langle \overline{u_i u_i} \rangle^{\frac{1}{2}}$ and λ_1 is a function of mixing length.*

The pressure-velocity gradient terms (i.e., the pressure redistribution terms) in equation 3 can be rewritten as

$$\left\langle \overline{u_i \frac{\partial p'}{\partial x_k}} \right\rangle + \left\langle \overline{u_k \frac{\partial p'}{\partial x_i}} \right\rangle = - \left\langle \overline{p' \frac{\partial u_i}{\partial x_k}} \right\rangle - \left\langle \overline{p' \frac{\partial u_k}{\partial x_i}} \right\rangle + \left\langle \overline{\frac{\partial p'}{\partial x_k} u_i} \right\rangle + \left\langle \overline{\frac{\partial p'}{\partial x_i} u_k} \right\rangle, \quad (9)$$

where

*In these equations, λ_1 through λ_7 are length scales, which contain a set of seven closure constants, i.e., $\lambda_k = a_k l$, where k is an arbitrary index 1–7 and l is the mixing length. Values for these closure constants are as follows: $a_1 = 0.39$, $a_2 = 0.85$, $a_3 = 16.57$, $a_4 = a_6 = 0.23$, $a_5 = 0.74$, and $a_7 = 10.10$ (11, 13–16).

$$\left\langle \overline{p' \frac{\partial u_i'}{\partial x_k}} \right\rangle + \left\langle \overline{p' \frac{\partial u_k'}{\partial x_i}} \right\rangle = -\frac{q}{3\lambda_2} \left[\left\langle \overline{u_i' u_k'} \right\rangle - \delta_{ik} \frac{q^2}{3} \right] + Cq^2 \left[\frac{\partial \langle \overline{u_i} \rangle}{\partial x_k} + \frac{\partial \langle \overline{u_k} \rangle}{\partial x_i} \right] , \quad (10)$$

and

$$\left\langle \overline{\frac{\partial p' u_i'}{\partial x_k}} \right\rangle + \left\langle \overline{\frac{\partial p' u_k'}{\partial x_i}} \right\rangle = 0 . \quad (11)$$

This is modeled according to the return-to-isotropy principle, as described by Mellor (14) and Donaldson (17). In equation 10, C is a constant whose value is about 0.077 (11).

Viscous dissipation is assumed isotropic and a function of local t.k.e. intensity. Viscous dissipation, as described by Katul and Albertson (11), is parameterized as

$$2\nu \left\langle \overline{\frac{\partial u_i' \partial u_k'}{\partial x_j \partial x_j}} \right\rangle = \frac{2}{3} \frac{q^3}{\lambda_3} \delta_{ik} . \quad (12)$$

In equation 4, the heat source term (S_θ), as described by Meyers and Paw U (12), is modeled as

$$S_\theta = 2A (\overline{\theta_l} - \overline{\theta}) / r_h . \quad (13)$$

Here, A (in units m^2m^{-3}) is the leaf area density, $(\overline{\theta_l} - \overline{\theta})$ is the mean leaf surface-to-ambient-air temperature difference, and r_h is the aerodynamic resistance to heat transfer. A 1-D radiative transfer and energy budget algorithm is incorporated into the 2-D model calculation to make it possible to determine the heat source for any time of day. To do this, the formulations outlined by Rachele and Tunick (18) are used to calculate the incoming total radiation at the canopy top as a function of latitude, longitude, day of year, and time of day (i.e., these input are needed to determine the solar declination, hour, and zenith angles). Then, the equations provided by Weiss and Norman (19) are used to calculate the spectral components for short-wave (i.e., direct beam and diffuse, visible and near-infrared) radiation as a function of the total downward short-wave flux at canopy top because extinction and reflection through the forest canopy are different for each. The remainder of the 1-D radiative transfer subroutine for the forest canopy (i.e., transmission, reflection, absorption, and emission of the solar flux) is derived from the formulations given in the texts by Campbell (20) and Campbell and Norman (21).

Returning now to equations 5 and 6, the triple-velocity-temperature products contained therein can be expressed in the form described by Mellor (14) and Mellor and Yamada (15, 16) as

$$\left\langle \overline{u_j' u_k' \theta'} \right\rangle = -q\lambda_4 \left[\frac{\partial \langle \overline{u_k' \theta'} \rangle}{\partial x_j} + \frac{\partial \langle \overline{u_j' \theta'} \rangle}{\partial x_k} \right] \quad (14)$$

and

$$\left\langle \overline{u_k' \theta'^2} \right\rangle = -q\lambda_6 \frac{\partial \langle \overline{\theta'^2} \rangle}{\partial x_k} . \quad (15)$$

In addition, the pressure interaction term can be modeled as

$$\left\langle \overline{p' \frac{\partial \theta'}{\partial x_j}} \right\rangle = -\frac{q}{3\lambda_5} \left\langle \overline{u'_j \theta'} \right\rangle - \frac{1}{3} \frac{g}{T} \left\langle \overline{\theta'^2} \right\rangle \delta_{j3} \quad . \quad (16)$$

Finally, the molecular dissipation of heat can be modeled as

$$2\kappa_T \left\langle \overline{\frac{\partial \theta'}{\partial x_k} \frac{\partial \theta'}{\partial x_k}} \right\rangle = \frac{2q}{\lambda_7} \left\langle \overline{\theta'^2} \right\rangle \quad . \quad (17)$$

This completes the basic equation set and modeling assumptions for the 2-D forest canopy model.

2.3 Second-Order Turbulence Closure Model for 2-D Forest Canopies

The 2-D computer model currently being developed is relatively unique. This is because higher-order closure models reported in the literature (e.g., 11–13, 22) have generally focused on estimates of 1-D, adiabatic wind flow, and turbulence within and above homogeneous (uniform) forest canopies. In contrast, the new model may be applied night or day to both uniform and nonuniform stands (and forest edges, possibly). The new model, which is based on the earlier works of Katul and Albertson (11), Meyers and Paw U (12), Wilson and Shaw (13), and Donaldson (17), calculates the 2-D, steady state, canopy wind flow, temperatures, turbulent variances, Reynolds stress, and heat flux. The parameterized 2-D model equations for continuity, the mean flow–longitudinal $\langle \bar{u} \rangle$, the mean flow–vertical $\langle \bar{w} \rangle$, Reynolds stress $\langle u'w' \rangle$, longitudinal $\langle \overline{u'^2} \rangle$, lateral $\langle \overline{v'^2} \rangle$, and vertical velocity $\langle \overline{w'^2} \rangle$ variances, the mean temperature $\langle \bar{\theta} \rangle$, vertical heat flux $\langle \overline{w'\theta'} \rangle$, horizontal heat flux $\langle \overline{u'\theta'} \rangle$, and the turbulent temperature variance $\langle \overline{\theta'^2} \rangle$, respectively, are as follows:

$$-\frac{1}{\langle \bar{\rho} \rangle} \frac{\partial \langle \bar{\rho} \rangle}{\partial t} = 0 = \frac{\partial \langle \bar{u} \rangle}{\partial x} + \frac{\partial \langle \bar{w} \rangle}{\partial z} \quad , \quad (18)$$

$$\frac{\partial \langle \bar{u} \rangle}{\partial t} = 0 = -\left\langle \overline{u \frac{\partial \langle \bar{u} \rangle}{\partial x}} \right\rangle - \left\langle \overline{w \frac{\partial \langle \bar{u} \rangle}{\partial z}} \right\rangle - \frac{\partial \langle \overline{u'^2} \rangle}{\partial x} - \frac{\partial \langle \overline{u'w'} \rangle}{\partial z} - \left\langle \overline{\frac{\partial p}{\partial x}} \right\rangle - C_d A |U| \langle \bar{u} \rangle \quad , \quad (19)$$

$$\frac{\partial \langle \bar{w} \rangle}{\partial t} = 0 = -\left\langle \overline{u \frac{\partial \langle \bar{w} \rangle}{\partial x}} \right\rangle - \left\langle \overline{w \frac{\partial \langle \bar{w} \rangle}{\partial z}} \right\rangle - \frac{\partial \langle \overline{u'w'} \rangle}{\partial x} - \frac{\partial \langle \overline{w'^2} \rangle}{\partial z} - \left\langle \overline{\frac{\partial p}{\partial z}} \right\rangle - C_d A |U| \langle \bar{w} \rangle + \frac{g\theta_0}{T} \quad , \quad (20)$$

$$\begin{aligned}
\frac{\partial \langle \overline{u'w'} \rangle}{\partial t} = 0 = & -\langle \overline{u} \rangle \frac{\partial \langle \overline{u'w'} \rangle}{\partial x} - \langle \overline{w} \rangle \frac{\partial \langle \overline{u'w'} \rangle}{\partial z} - \langle \overline{u'w'} \rangle \frac{\partial \langle \overline{u} \rangle}{\partial x} - \langle \overline{w'^2} \rangle \frac{\partial \langle \overline{u} \rangle}{\partial z} - \langle \overline{u'^2} \rangle \frac{\partial \langle \overline{w} \rangle}{\partial x} - \langle \overline{u'w'} \rangle \frac{\partial \langle \overline{w} \rangle}{\partial z} \\
& + \frac{\partial}{\partial x} \left(q\lambda_1 \left(2 \frac{\partial \langle \overline{u'w'} \rangle}{\partial x} + \frac{\partial \langle \overline{u'^2} \rangle}{\partial z} \right) \right) + \frac{\partial}{\partial z} \left(q\lambda_1 \left(\frac{\partial \langle \overline{w'^2} \rangle}{\partial x} + 2 \frac{\partial \langle \overline{u'w'} \rangle}{\partial z} \right) \right) + \frac{g}{T} \langle \overline{u'\theta'} \rangle - \frac{q}{3\lambda_2} \langle \overline{u'w'} \rangle \\
& + Cq^2 \left(\frac{\partial \langle \overline{u} \rangle}{\partial z} + \frac{\partial \langle \overline{w} \rangle}{\partial x} \right) + \langle \overline{w} \rangle C_d A |\overline{U}| \langle \overline{u} \rangle + \langle \overline{u} \rangle C_d A |\overline{U}| \langle \overline{w} \rangle ,
\end{aligned} \tag{21}$$

$$\begin{aligned}
\frac{\partial \langle \overline{u'^2} \rangle}{\partial t} = 0 = & -\langle \overline{u} \rangle \frac{\partial \langle \overline{u'^2} \rangle}{\partial x} - \langle \overline{w} \rangle \frac{\partial \langle \overline{u'^2} \rangle}{\partial z} - 2 \langle \overline{u'^2} \rangle \frac{\partial \langle \overline{u} \rangle}{\partial x} - 2 \langle \overline{u'w'} \rangle \frac{\partial \langle \overline{u} \rangle}{\partial z} + \frac{\partial}{\partial x} \left(3q\lambda_1 \frac{\partial \langle \overline{u'^2} \rangle}{\partial x} \right) \\
& + \frac{\partial}{\partial z} \left(q\lambda_1 \left(2 \frac{\partial \langle \overline{u'w'} \rangle}{\partial x} + \frac{\partial \langle \overline{u'^2} \rangle}{\partial z} \right) \right) - \frac{q}{3\lambda_2} \left(\langle \overline{u'^2} \rangle - \frac{q^2}{3} \right) + 2Cq^2 \frac{\partial \langle \overline{u} \rangle}{\partial x} + 2C_d A |\overline{U}| \langle \overline{u} \rangle^2 - \frac{2}{3} \frac{q^3}{\lambda_3} ,
\end{aligned} \tag{22}$$

$$\frac{\partial \langle \overline{w'^2} \rangle}{\partial t} = 0 = -\langle \overline{u} \rangle \frac{\partial \langle \overline{w'^2} \rangle}{\partial x} - \langle \overline{w} \rangle \frac{\partial \langle \overline{w'^2} \rangle}{\partial z} + \frac{\partial}{\partial x} \left(q\lambda_1 \frac{\partial \langle \overline{w'^2} \rangle}{\partial x} \right) + \frac{\partial}{\partial z} \left(q\lambda_1 \frac{\partial \langle \overline{w'^2} \rangle}{\partial z} \right) - \frac{q}{3\lambda_2} \left(\langle \overline{w'^2} \rangle - \frac{q^2}{3} \right) - \frac{2}{3} \frac{q^3}{\lambda_3} , \tag{23}$$

$$\begin{aligned}
\frac{\partial \langle \overline{w'^2} \rangle}{\partial t} = 0 = & -\langle \overline{u} \rangle \frac{\partial \langle \overline{w'^2} \rangle}{\partial x} - \langle \overline{w} \rangle \frac{\partial \langle \overline{w'^2} \rangle}{\partial z} - 2 \langle \overline{u'w'} \rangle \frac{\partial \langle \overline{w} \rangle}{\partial x} - 2 \langle \overline{w'^2} \rangle \frac{\partial \langle \overline{w} \rangle}{\partial z} + \frac{\partial}{\partial x} \left(q\lambda_1 \left(2 \frac{\partial \langle \overline{u'w'} \rangle}{\partial z} + \frac{\partial \langle \overline{w'^2} \rangle}{\partial x} \right) \right) \\
& + \frac{\partial}{\partial z} \left(3q\lambda_1 \frac{\partial \langle \overline{w'^2} \rangle}{\partial z} \right) + 2 \frac{g}{T} \langle \overline{w'\theta'} \rangle - \frac{q}{3\lambda_2} \left(\langle \overline{w'^2} \rangle - \frac{q^2}{3} \right) + 2Cq^2 \frac{\partial \langle \overline{w} \rangle}{\partial z} + 2C_d A |\overline{U}| \langle \overline{w} \rangle^2 - \frac{2}{3} \frac{q^3}{\lambda_3} ,
\end{aligned} \tag{24}$$

$$\frac{d \langle \overline{\theta} \rangle}{dt} = 0 = -\langle \overline{u} \rangle \frac{\partial \langle \overline{\theta} \rangle}{\partial x} - \langle \overline{w} \rangle \frac{\partial \langle \overline{\theta} \rangle}{\partial z} - \frac{\partial \langle \overline{u'\theta'} \rangle}{\partial x} - \frac{\partial \langle \overline{w'\theta'} \rangle}{\partial z} + S_\theta , \tag{25}$$

$$\begin{aligned}
\frac{\partial \langle \overline{w'\theta'} \rangle}{\partial t} = 0 = & -\langle \overline{u} \rangle \frac{\partial \langle \overline{w'\theta'} \rangle}{\partial x} - \langle \overline{w} \rangle \frac{\partial \langle \overline{w'\theta'} \rangle}{\partial z} - \langle \overline{u'w'} \rangle \frac{\partial \langle \overline{\theta} \rangle}{\partial x} - \langle \overline{w'^2} \rangle \frac{\partial \langle \overline{\theta} \rangle}{\partial z} - \langle \overline{u'\theta'} \rangle \frac{\partial \langle \overline{w} \rangle}{\partial x} - \langle \overline{w'\theta'} \rangle \frac{\partial \langle \overline{w} \rangle}{\partial z} \\
& + \frac{\partial}{\partial x} \left(q\lambda_4 \left(\frac{\partial \langle \overline{u'\theta'} \rangle}{\partial z} + \frac{\partial \langle \overline{w'\theta'} \rangle}{\partial x} \right) \right) + \frac{\partial}{\partial z} \left(2q\lambda_4 \frac{\partial \langle \overline{w'\theta'} \rangle}{\partial z} \right) + \frac{2}{3} \frac{g}{T} \langle \overline{\theta'^2} \rangle - \frac{q}{3\lambda_5} \langle \overline{w'\theta'} \rangle ,
\end{aligned} \tag{26}$$

$$\begin{aligned}
\frac{\partial \langle \overline{u' \theta'} \rangle}{\partial t} = 0 = & -\langle \overline{u} \rangle \frac{\partial \langle \overline{u' \theta'} \rangle}{\partial x} - \langle \overline{w} \rangle \frac{\partial \langle \overline{u' \theta'} \rangle}{\partial z} - \langle \overline{u^2} \rangle \frac{\partial \langle \overline{\theta} \rangle}{\partial x} - \langle \overline{u' w'} \rangle \frac{\partial \langle \overline{\theta} \rangle}{\partial z} - \langle \overline{u' \theta'} \rangle \frac{\partial \langle \overline{u} \rangle}{\partial x} - \langle \overline{w' \theta'} \rangle \frac{\partial \langle \overline{u} \rangle}{\partial z} \\
& + \frac{\partial}{\partial x} \left(2q\lambda_4 \frac{\partial \langle \overline{u' \theta'} \rangle}{\partial x} \right) + \frac{\partial}{\partial z} \left(q\lambda_4 \left(\frac{\partial \langle \overline{w' \theta'} \rangle}{\partial x} + \frac{\partial \langle \overline{u' \theta'} \rangle}{\partial z} \right) \right) - \frac{q}{3\lambda_5} \langle \overline{u' \theta'} \rangle,
\end{aligned} \tag{27}$$

and

$$\begin{aligned}
\frac{\partial \langle \overline{\theta'^2} \rangle}{\partial t} = 0 = & -\langle \overline{u} \rangle \frac{\partial \langle \overline{\theta'^2} \rangle}{\partial x} - \langle \overline{w} \rangle \frac{\partial \langle \overline{\theta'^2} \rangle}{\partial z} - 2\langle \overline{u' \theta'} \rangle \frac{\partial \langle \overline{\theta} \rangle}{\partial x} - 2\langle \overline{w' \theta'} \rangle \frac{\partial \langle \overline{\theta} \rangle}{\partial z} \\
& + \frac{\partial}{\partial x} \left(q\lambda_6 \frac{\partial \langle \overline{\theta'^2} \rangle}{\partial x} \right) + \frac{\partial}{\partial z} \left(q\lambda_6 \frac{\partial \langle \overline{\theta'^2} \rangle}{\partial z} \right) - \frac{2q}{\lambda_7} \langle \overline{\theta'^2} \rangle.
\end{aligned} \tag{28}$$

In the model, mean pressure is assumed approximately hydrostatic. In contrast, the kinematic (fluctuation) pressure $\langle \overline{p} \rangle$ is determined, as discussed in the text by Ferziger and Perić (23), by taking the divergence of the mean flow equations, i.e.,

$$\begin{aligned}
\frac{\partial}{\partial x} \left(\frac{\partial \langle \overline{u} \rangle}{\partial t} \right) = 0 = & -\frac{\partial}{\partial x} \left\langle \overline{u} \frac{\partial \langle \overline{u} \rangle}{\partial x} \right\rangle - \frac{\partial}{\partial x} \left\langle \overline{w} \frac{\partial \langle \overline{u} \rangle}{\partial z} \right\rangle - \frac{\partial^2 \langle \overline{u^2} \rangle}{\partial x^2} - \frac{\partial}{\partial x} \left(\frac{\partial \langle \overline{u' w'} \rangle}{\partial z} \right) \\
& - \left\langle \frac{\partial^2 \overline{p}}{\partial x^2} \right\rangle - C_d A |U| \frac{\partial \langle \overline{u} \rangle}{\partial x},
\end{aligned} \tag{29}$$

and

$$\begin{aligned}
\frac{\partial}{\partial z} \left(\frac{\partial \langle \overline{w} \rangle}{\partial t} \right) = 0 = & -\frac{\partial}{\partial z} \left\langle \overline{u} \frac{\partial \langle \overline{w} \rangle}{\partial x} \right\rangle - \frac{\partial}{\partial z} \left\langle \overline{w} \frac{\partial \langle \overline{w} \rangle}{\partial z} \right\rangle - \frac{\partial}{\partial z} \left(\frac{\partial \langle \overline{u' w'} \rangle}{\partial x} \right) - \frac{\partial^2 \langle \overline{w^2} \rangle}{\partial z^2} \\
& - \left\langle \frac{\partial^2 \overline{p}}{\partial z^2} \right\rangle + \frac{g}{T} \frac{\partial \langle \overline{\theta} \rangle}{\partial z} - C_d A |U| \frac{\partial \langle \overline{w} \rangle}{\partial z},
\end{aligned} \tag{30}$$

which, after some rearranging and cancellation of terms due to continuity, yields Poisson's equation (i.e., pressure-velocity coupling) as

$$\left\langle \frac{\partial^2 \overline{p}}{\partial z^2} \right\rangle + \left\langle \frac{\partial^2 \overline{p}}{\partial x^2} \right\rangle = -\frac{\partial^2 \langle \overline{u^2} \rangle}{\partial x^2} - \frac{\partial}{\partial x} \left(\frac{\partial \langle \overline{u' w'} \rangle}{\partial z} \right) - \frac{\partial}{\partial z} \left(\frac{\partial \langle \overline{u' w'} \rangle}{\partial x} \right) - \frac{\partial^2 \langle \overline{w^2} \rangle}{\partial z^2} + \frac{g}{T} \frac{\partial \langle \overline{\theta} \rangle}{\partial z}. \tag{31}$$

Also, note that the lateral velocity variance $\langle \overline{v'^2} \rangle$ is calculated in the current 2-D model

(equation 23) to support the turbulence (t.k.e.) closure approximations for the triple product and dissipation terms.

2.4 Numerical Methods

A computational grid consisting of 10×60 points is chosen, where the horizontal grid spacing (Δx) is 50 m and the vertical grid spacing (Δz) is 0.5 m. Hence, the model domain is 500×30 m. Vertical derivatives are solved using a lower-order central differencing scheme (23). The first derivatives can be expressed as

$$\frac{\partial \phi_{(i,j)}}{\partial z} = \frac{\phi_{(i,j+1)} - \phi_{(i,j-1)}}{2\Delta z} , \quad (32)$$

and the second derivatives as

$$\frac{\partial^2 \phi_{(i,j)}}{\partial z^2} = \frac{\phi_{(i,j-1)} - 2\phi_{(i,j)} + \phi_{(i,j+1)}}{(\Delta z)^2} . \quad (33)$$

Here, i is the horizontal grid index and j is the vertical grid index. In contrast, the horizontal derivatives are solved using a lower-order upwind differencing scheme (23), such that the first derivatives are computed as

$$\frac{\partial \phi_{(i,j)}}{\partial x} = \frac{\phi_{(i,j)} - \phi_{(i-1,j)}}{\Delta x} , \quad (34)$$

and the second derivatives are given as

$$\frac{\partial^2 \phi_{(i,j)}}{\partial x^2} = \frac{\phi_{(i,j)} - 2\phi_{(i-1,j)} + \phi_{(i-2,j)}}{(\Delta x)^2} . \quad (35)$$

A set of simultaneous equations for each of 12 computed variables is then solved iteratively using the Thomas algorithm, a tridiagonal matrix solver (24). In addition, the solution implements a relaxation scheme for all the computed variables, similar to that described by Wilson (22), i.e.,

$$\phi = a\phi^n + (1-a)\phi^{n-1} , \quad (36)$$

where $a = 0.05$, n is the current iteration, and $n - 1$ is the previous iteration. The relaxation scheme primarily affects the rate at which the solution converges, not how well the solution converges.

Then, based on the earlier works of Meyers and Paw U (12) and Katul and Albertson (11), the following (model) top and bottom boundary conditions are applied:

At $z = 0$:

$$\langle \bar{u} \rangle = \langle \bar{w} \rangle = 0 ; \quad \langle \bar{\theta} \rangle = 303.15 ;$$

$$\langle \bar{p} \rangle = 0 ;$$

$$\langle \overline{u'w'} \rangle = 0 ; \quad \langle \overline{w'\theta'} \rangle = \langle \overline{u'\theta'} \rangle = 0 ;$$

$$\langle \overline{u^2} \rangle = \langle \overline{v^2} \rangle = \langle \overline{w^2} \rangle = \langle \overline{\theta^2} \rangle = 0 ;$$

$$u_* = \left| \langle \overline{u'w'} \rangle_{(i,2)} \right|^{0.5} \text{ (friction velocity at } z = 2\Delta z);$$

$$\theta_* = \frac{\langle \overline{w'\theta'} \rangle_{(i,2)}}{u_*} \text{ (potential temperature scaling constant at } z = 2\Delta z);$$

$$\frac{\partial \langle \overline{u} \rangle}{\partial z} = \frac{u_*}{k 2\Delta z} \quad \text{and} \quad \frac{\partial \langle \overline{\theta} \rangle}{\partial z} = \frac{\theta_*}{k 2\Delta z} \quad (k = 0.4 \text{ is von Karman's constant});$$

$$\frac{\partial \langle \overline{w} \rangle}{\partial z} = 0 \quad \text{and} \quad \frac{\partial \langle \overline{p} \rangle}{\partial z} = 0 .$$

At $z = 30 \text{ m}$:

$$\frac{\partial \langle \overline{u} \rangle}{\partial z} = \frac{u_*}{k(z-d)} \quad \text{and} \quad \frac{\partial \langle \overline{\theta} \rangle}{\partial z} = \frac{\theta_*}{k(z-d)}$$

(d is displacement height ($d \approx \frac{2}{3}h$) and h is canopy height);

$$u_* = \frac{k \left(U^{top} - \langle \overline{u} \rangle_{(i,h+10\Delta z)} \right)}{\log \left(\frac{z-d}{h+10\Delta z-d} \right)} \quad (U^{top} = 7.0 \text{ ms}^{-1});$$

$$Q_h = \int_0^h S_\theta \, dz \text{ (kinematic heat flux, } Q_h = \langle \overline{w'\theta'} \rangle);$$

$$\theta_* = \frac{-Q_h}{u_*} \text{ (potential temperature scaling constant);}$$

$$\frac{\partial \langle \overline{w} \rangle}{\partial z} = 0 \quad \text{and} \quad \frac{\partial \langle \overline{p} \rangle}{\partial z} = 0 ;$$

$$\langle \overline{u'w'} \rangle = -u_*^2 ; \quad \langle \overline{w'\theta'} \rangle = Q_h ; \quad \text{and} \quad \langle \overline{u'\theta'} \rangle = -3.0 \, Q_h ;$$

$$\langle \overline{u^2} \rangle = 3.5 \, u_*^2 ; \quad \langle \overline{v^2} \rangle = 1.5 \, u_*^2 ; \quad \langle \overline{w^2} \rangle = 1.5 \, u_*^2 ; \quad \text{and} \quad \langle \overline{\theta^2} \rangle = 4.0 \, \theta_*^2 .$$

In addition, zero-gradient conditions are assumed at the lateral boundaries. However, a weighted smoother, similar to that proposed by Mahrer and Pielke (25), is applied to the first three and last three horizontal grid points to reduce undesired boundary effects, i.e.,

$$\phi_{(i,j)} = 0.5\phi_{(i,j)} + 0.25(\phi_{(i+1,j)} + \phi_{(i-1,j)}) \quad . \quad (37)$$

Finally, lower-order Newton-Cotes formulas for numerical integration, i.e., the trapezoidal rule and Simpson's one-third rule, are applied to derive the wind flow streamlines.

2.5 Forest Canopy Architecture

As shown in sections 2.2 and 2.3, canopy architecture plays an important role in defining the momentum and heat flux divergence through the forest layer. Following the discussions by Massman (26) and Meyers et al. (27), it was suggested that forest canopies may conform to one of three general leaf area distribution profiles, as shown in Figure 1. It is clear that leaf area distributions are not always symmetric about the layer of maximum foliage density (like profile-1) but may be more often skewed upward toward the top of the forest canopy. By definition, leaf

area index is $LAI = \int_0^h A(z) dz$, where $A(z)$ is the leaf area density through the small vertical layer

between z and $z + \Delta z$ per unit surface area of ground below (28). Values for leaf area index for forests vary but have been reported most often in the range $LAI = 1$ to 5 (29). In section 3, 2-D model results will be shown for the case corresponding to profile-2. Also, in this study $LAI = 3.0$.

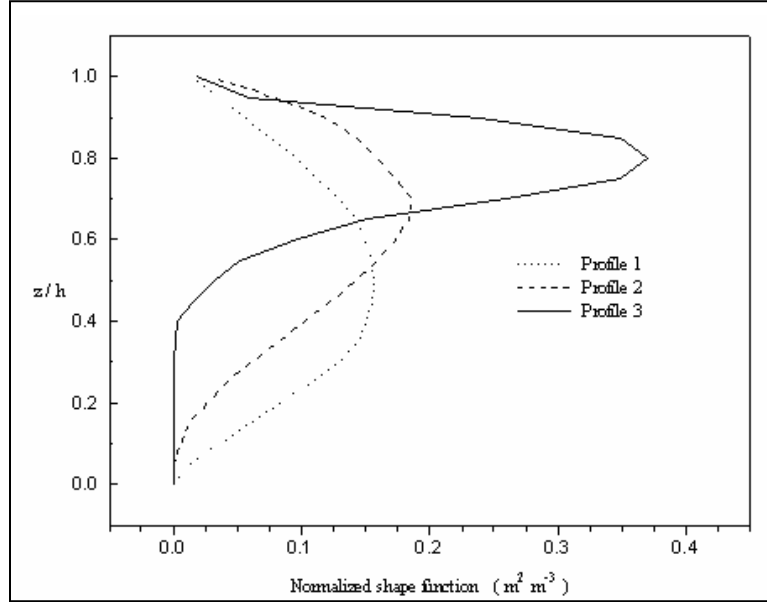


Figure 1. Normalized vertical profiles of leaf area density for forest canopies.

3. Model Results

3.1 Uniform Forest Stands

In this section, several initial model results are presented for a 2-D uniform forest stand. Figure 2 shows the calculated fields for horizontal wind velocity, $\langle \bar{u} \rangle$, in units ms^{-1} , and air temperature, $\langle \bar{\theta} \rangle$, in units $^{\circ}\text{C}$. For this example, upper level (i.e., model top) wind velocity is

$u_{max} = 7.0 \text{ ms}^{-1}$, leaf area index is $LAI = 3$, and forest canopy height is $h = 10 \text{ m}$. In contrast, Figure 3 shows individual profiles for wind velocity and air temperature derived from the current 2-D calculation in comparison to profiles derived from an earlier 1-D modeling study (1, 2). Profile results from the 1-D and 2-D models agree reasonably well. Small differences are due (possibly) to the expanded numerical grid. Finally, Figure 4 shows some spurious oscillations that result when $\Delta x = 20 \text{ m}$. Here, it is likely that the solution is unstable because $\Delta x/Z(N) < 1$, where $Z(N)$ is the height at the model top. Based on an analysis of the equation set and several additional calculations (not shown), this condition for stability appears to be valid. The computed variable in Figure 4 is horizontal wind velocity, $\langle \bar{u} \rangle$, in units ms^{-1} .

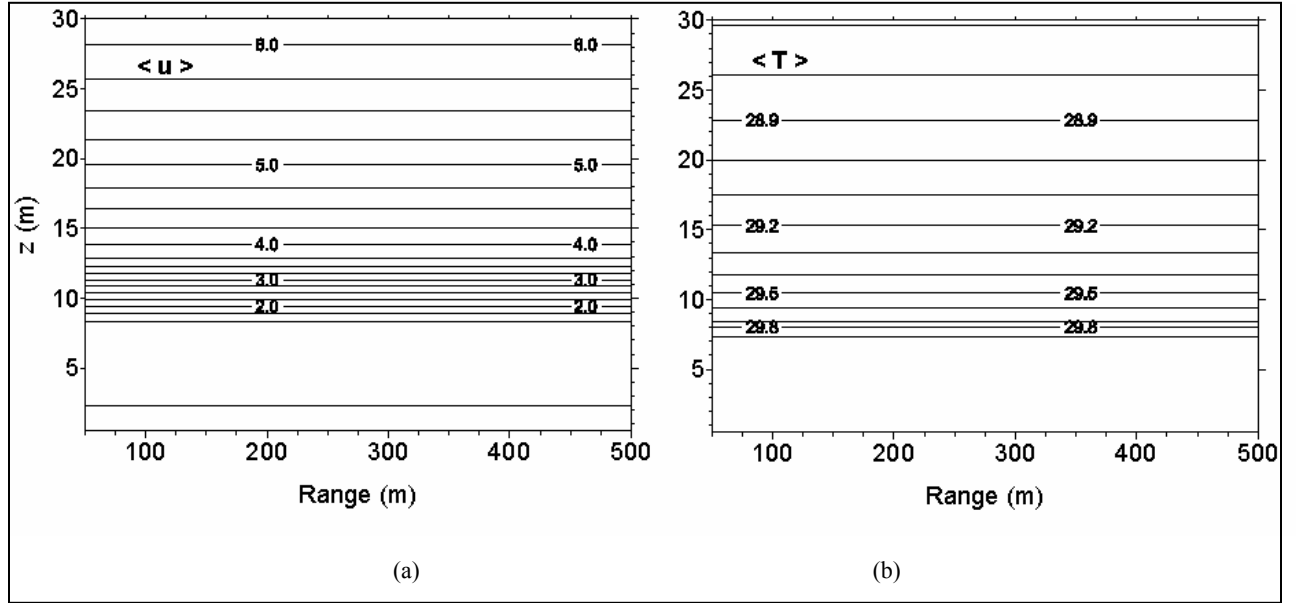


Figure 2. Model results for uniform forest stands: (a) horizontal wind velocity, $\langle \bar{u} \rangle$, in units ms^{-1} , and (b) air temperature, $\langle \bar{\theta} \rangle$, in units $^{\circ}\text{C}$. For this example, canopy height (h) is 10 m.

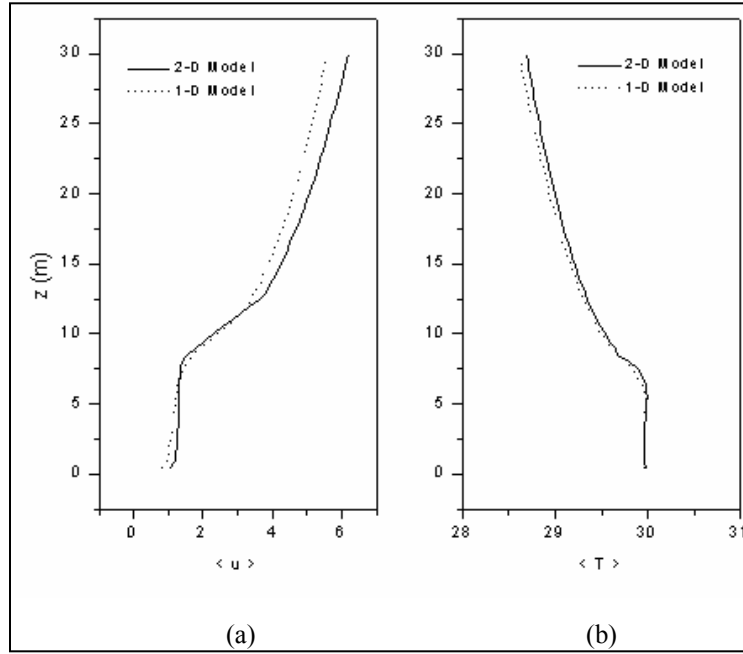


Figure 3. Profiles of horizontal wind velocity ($\langle \bar{u} \rangle$, in units ms^{-1}) and air temperature ($\langle \bar{\theta} \rangle$, in units $^{\circ}\text{C}$) derived from the current 2-D calculation shown in comparison to 1-D profiles derived from an earlier study.

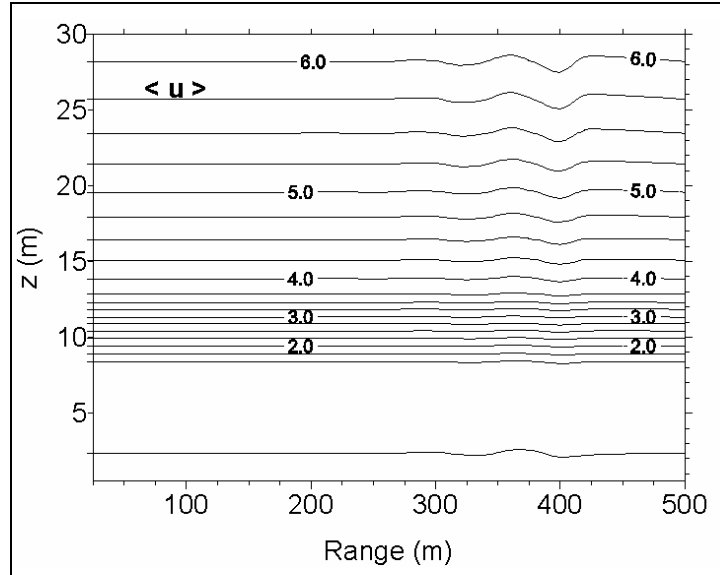


Figure 4. Spurious oscillations due to numerical instability in the 2-D model results for uniform forest stands. The computed variable is horizontal wind velocity, $\langle \bar{u} \rangle$, in units ms^{-1} .

3.2 Nonuniform Forest Stands

Figures 5–7 show the current 2-D model results for a nonuniform forest stand, i.e., which contains a single step change in canopy height. The computed variables in Figure 5 are horizontal wind velocity, $\langle \bar{u} \rangle$, in units ms^{-1} , and the wind flow streamlines. A single step change in canopy height (h) at one grid increment past the midpoint (i.e., $X/2 + \Delta x$) is shown via open rectangles, where $h = 8 \text{ m}$ on the left side and $h = 10 \text{ m}$ on the right side. The computed variables in Figure 6 are vertical wind velocity, $\langle \bar{w} \rangle$, in units ms^{-1} , and kinematic (fluctuation) pressure $\langle \bar{p} \rangle$, in units $\text{m}^{-2}\text{s}^{-2}$. The computed variables in Figure 7 are air temperature, $\langle \bar{\theta} \rangle$, in units $^{\circ}\text{C}$, and the effective speed of sound, $\langle \bar{C}_{\text{eff}} \rangle$, in units ms^{-1} . Finally, Figure 8 shows spurious oscillations that result when $\Delta x = 20 \text{ m}$ instead of $\Delta x = 50 \text{ m}$. Here again, a computational instability is brought about (possibly) because $\Delta x/Z(N) < 1$.

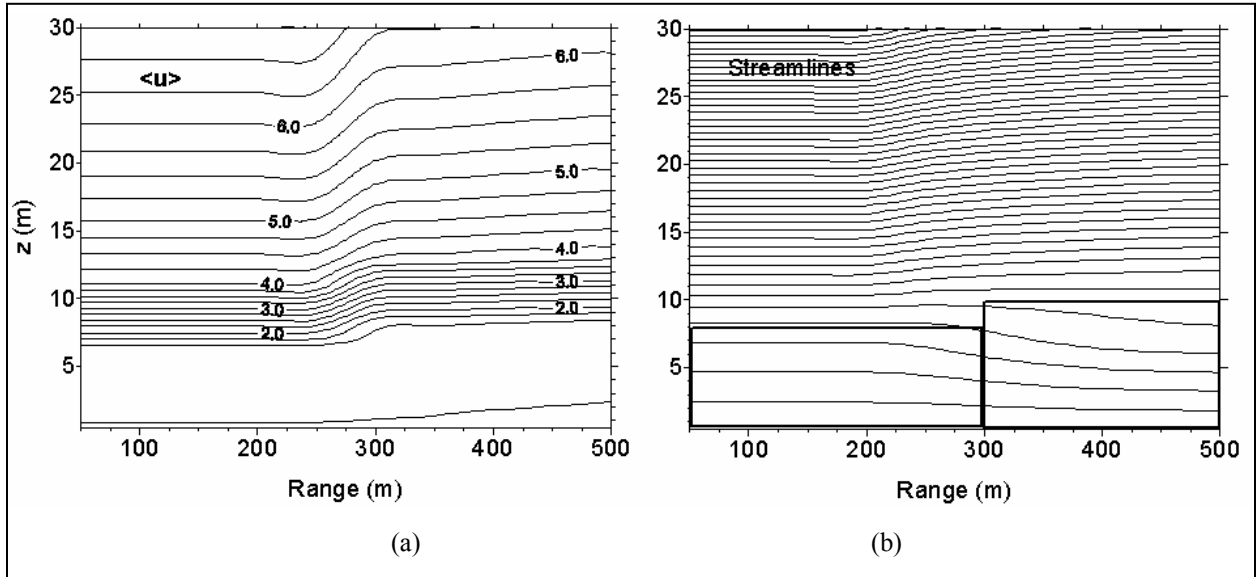


Figure 5. Model results for nonuniform forest stands, i.e., those that contain a single step change in canopy height: (a) horizontal wind velocity, $\langle \bar{u} \rangle$, in units ms^{-1} , and (b) wind flow streamlines. A single step change in canopy height at $X/2 + \Delta x$ is shown using open rectangles, where $h = 8 \text{ m}$ on the left side and $h = 10 \text{ m}$ on the right side.

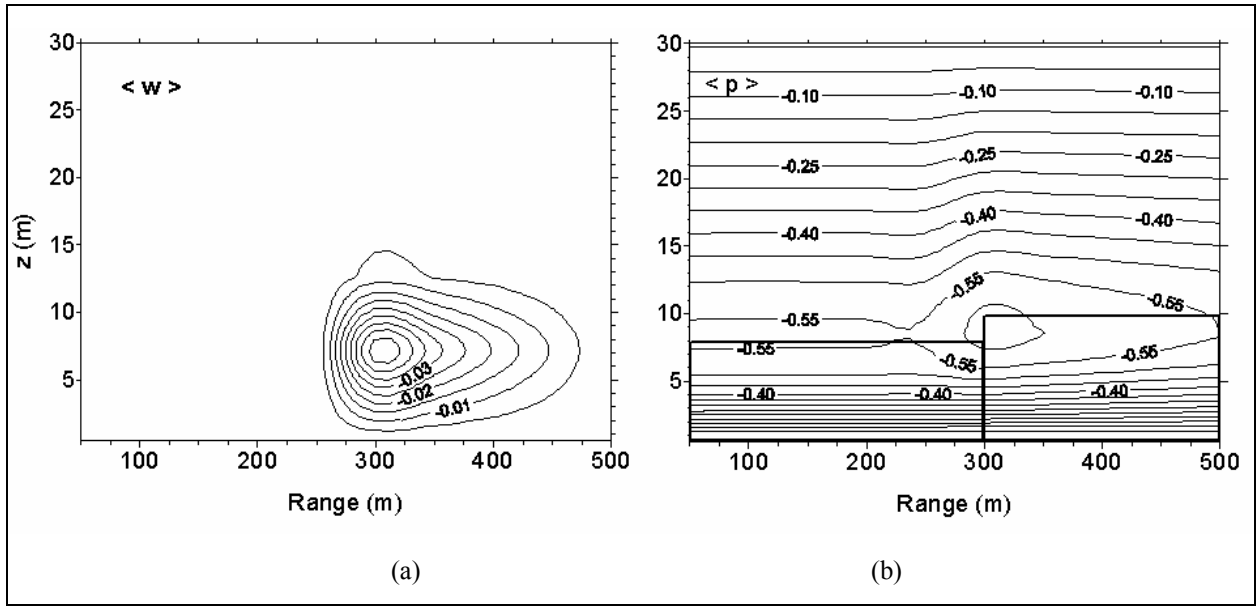


Figure 6. Model results for nonuniform forest stands: (a) vertical wind velocity, $\langle w \rangle$, in units ms^{-1} and (b) kinematic (fluctuation) pressure $\langle p \rangle$, in units $\text{m}^{-2}\text{s}^{-2}$. A single step change in canopy height occurs at $X/2 + \Delta x$, where $h = 8$ m on the left side and $h = 10$ m on the right side.

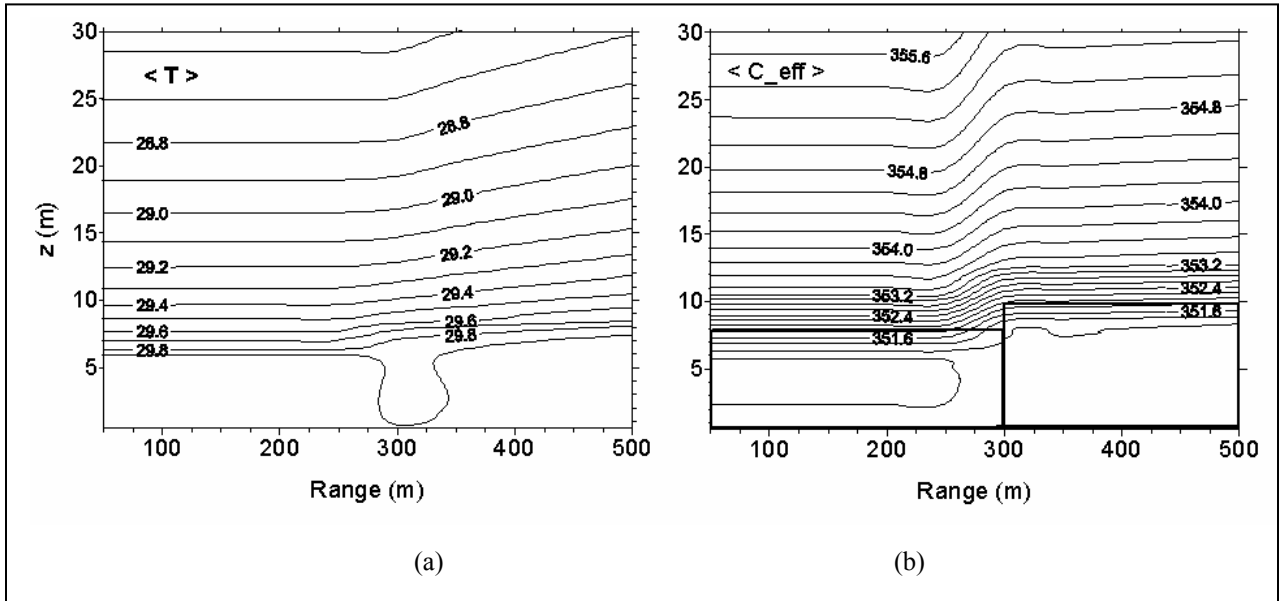


Figure 7. Model results for nonuniform forest stands: (a) air temperature, $\langle T \rangle$, in units $^{\circ}\text{C}$ and (b) effective speed of sound, $\langle C_{\text{eff}} \rangle$, in units ms^{-1} . A single step change in canopy height occurs at $X/2 + \Delta x$, where $h = 8$ m on the left side and $h = 10$ m on the right side.

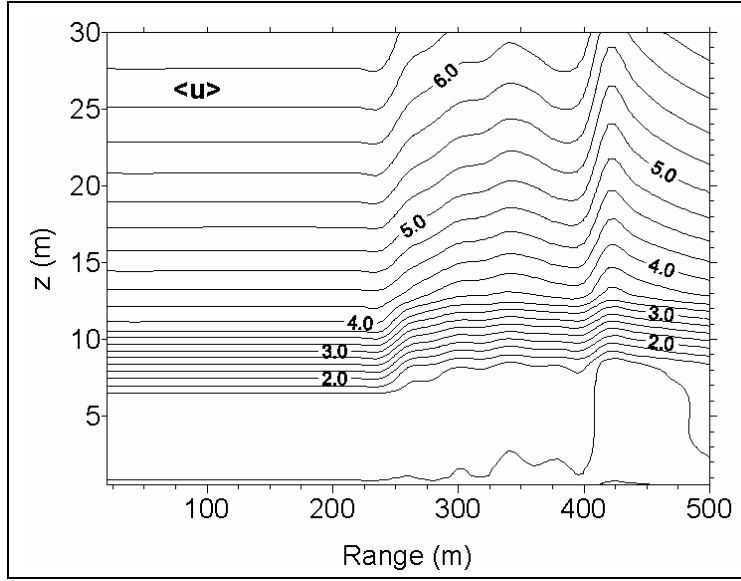


Figure 8. Spurious oscillations due to numerical instability in the 2-D model results for nonuniform forest stands. The computed variable is horizontal wind velocity, $\langle \bar{u} \rangle$, in units ms^{-1} .

Figures 9–11 show the current 2-D model results for a second nonuniform forest stand. In this example, a larger step in canopy height is incorporated at the lower boundary, where $h = 4$ m on the left side and $h = 10$ m on the right side. The computed variables in Figure 9 are horizontal wind velocity, $\langle \bar{u} \rangle$, in units ms^{-1} , and the wind flow streamlines. The computed variables in Figure 10 are vertical wind velocity, $\langle \bar{w} \rangle$, in units ms^{-1} , and kinematic (fluctuation) pressure $\langle \bar{p} \rangle$, in units $\text{m}^{-2}\text{s}^{-2}$. The computed variables in Figure 11 are air temperature, $\langle \bar{\theta} \rangle$, in units $^{\circ}\text{C}$, and the effective speed of sound, $\langle \bar{C}_{\text{eff}} \rangle$, in units ms^{-1} . Finally, Figure 12 shows that care needs to be taken when applying numerical (integration) schemes across sharp discontinuities (e.g., to calculate the streamlines). Here, the use of Simpson's one-third rule for both integrals, i.e., $\int d\psi = -\int w dx + \int u dz$, resulted in a computational instability (i.e., $2\Delta x$ numerical waves). Upon further analysis, these were found to be contained mainly in the solution to $-\int w dx$. A stable solution was later obtained by applying a simpler trapezoidal rule to solve this integral. Note that while $\Delta x = 50$ m in Figure 12, the number of horizontal grid points is expanded (i.e., $MPT = 40$).

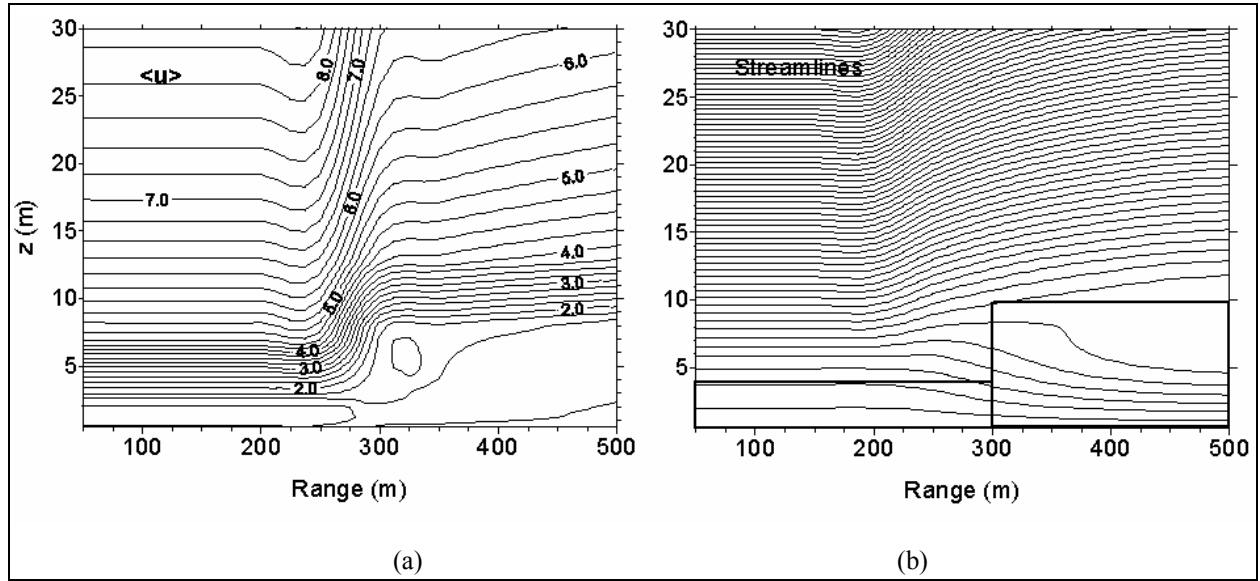


Figure 9. Model results for nonuniform forest stands, i.e., those that contain a single step change in canopy height: (a) horizontal wind velocity, $\langle u \rangle$, in units ms^{-1} , and (b) wind flow streamlines. A single step change in canopy height at $X/2 + \Delta x$ is shown using open rectangles, where $h = 4$ m on the left side and $h = 10$ m on the right side.

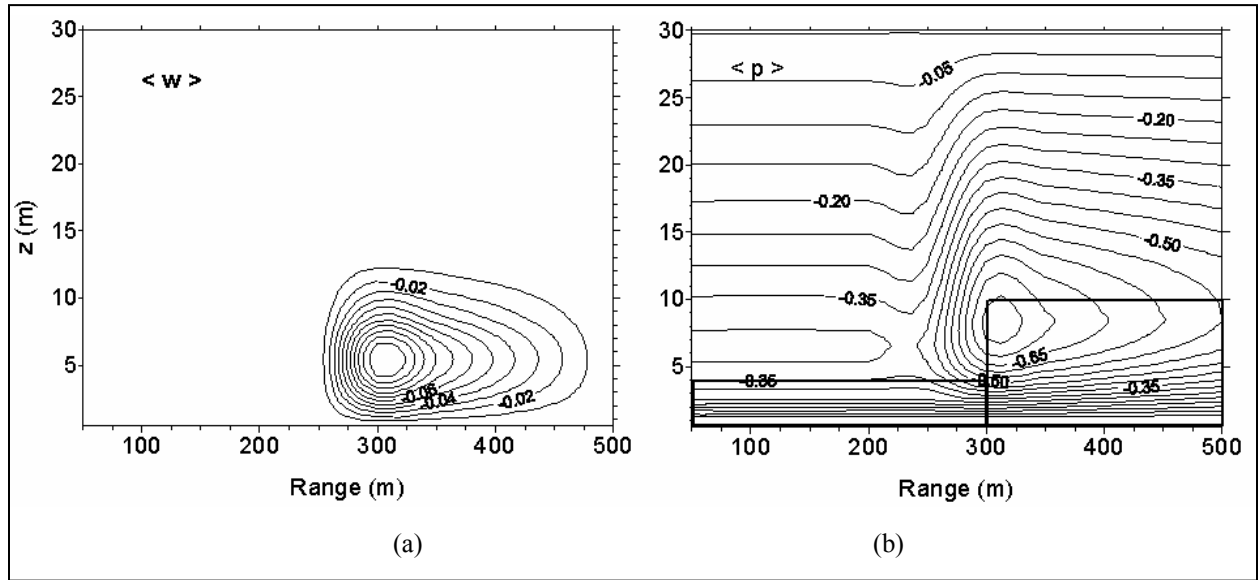


Figure 10. Model results for nonuniform forest stands: (a) vertical wind velocity, $\langle w \rangle$, in units ms^{-1} , and (b) kinematic (fluctuation) pressure $\langle p \rangle$, in units m^2s^{-2} . A single step change in canopy height occurs at $X/2 + \Delta x$, where $h = 4$ m on the left side and $h = 10$ m on the right side.

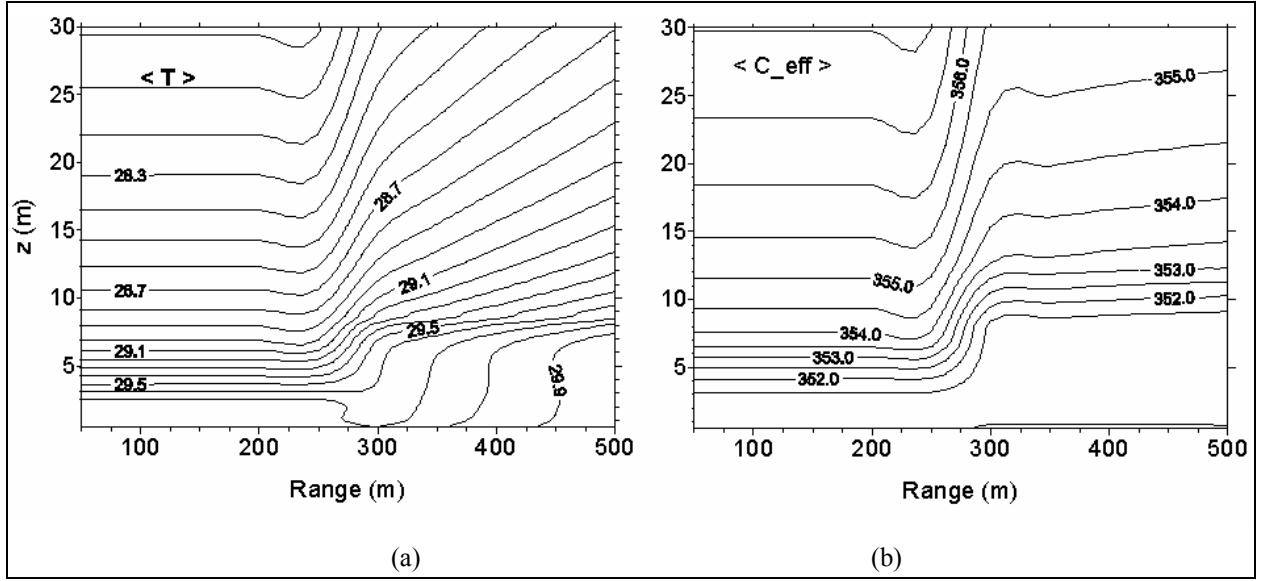


Figure 11. Model results for nonuniform forest stands: (a) air temperature, $\langle \bar{\theta} \rangle$, in units $^{\circ}\text{C}$, and (b) effective speed of sound, $\langle \bar{C}_{\text{eff}} \rangle$, in units ms^{-1} . A single step change in canopy height occurs at $X/2 + \Delta x$, where $h = 4$ m on the left side and $h = 10$ m on the right side.

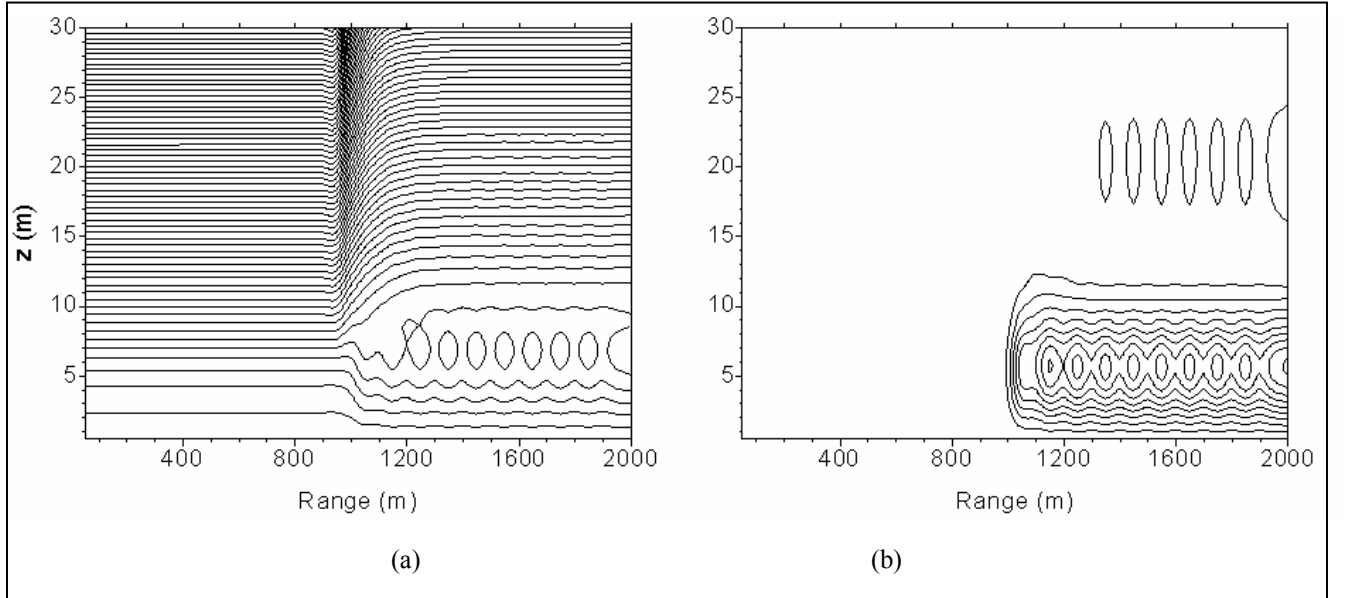


Figure 12. Numerical instability, i.e., $2\Delta x$ waves, in the computation of wind flow streamlines for nonuniform forest stands: (a) $\int d\psi = -\int w dx + \int u dz$ and (b) $\int d\psi = -\int w dx$ only. A single step change in canopy height occurs at $X/2 + \Delta x$, where $h = 4$ m on the left side and $h = 10$ m on the right side.

4. Summary and Conclusions

A new and relatively unique, physics-based, meteorological computer model for 2-D forest canopy wind flow, temperature, and turbulence calculations has been developed. The current 2-D model is based on the same basic conservation-law equations and (second-order turbulence closure) modeling assumptions that were implemented in an earlier 1-D model study to mathematically represent the mechanical and thermodynamic influences on the speed of sound in the forest environment. The 2-D computer model has been implemented in Fortran. Valid numerical techniques from earlier works have been applied to solve for each of twelve computed variables, to include the mean flow vertical velocity and the kinematic (fluctuation) pressure. The horizontal derivatives were solved using lower-order, upwind differencing. The vertical derivatives were solved using lower-order, central differencing. Second-order, ordinary differential equations for the profiles were solved using a tridiagonal matrix algorithm. Thus, several satisfactory solutions were achieved for uniform and nonuniform forest stands (for coarse horizontal grid spacing, i.e., $\Delta x = 50$ m). In addition, a valid condition for numerical stability was determined, as $\Delta x/Z(N) > 1$.

In future modeling works, we will continue to investigate these and alternate numerical schemes, which are accurate, fast, and robust, to solve the computed fields within and above a realistic forest canopies, particularly those containing sharp discontinuities at the lower boundary (e.g., forest edges [30]). Also, the presence of hills may significantly alter the flow field inside canopies (31). Most turbulence models, including the model described herein, are for flat surfaces. Therefore, additional 2-D forest canopy models may begin to consider uneven terrain.

5. References

1. Tunick, A. *Coupling Meteorology to Acoustics in Forests*. Presented at the 23rd Army Science Conference, sponsored by the Assistant Secretary of the Army (Acquisition, Logistics and Technology), Orlando, FL, 2–5 December 2002; <http://www.asc2002.com/manuscripts/E/EO-03.PDF> (accessed Jun 2003).
2. Tunick, A. Calculating the Micrometeorological Influences on the Speed of Sound Through the Atmosphere in Forests. *Journal of the Acoustical Society of America*, submitted for publication 2003.
3. Noble, J. M. *User's Manual for the Microsoft Window Edition of the Scanning Fast-Field Program (SCAFFIP) Version 3.0*; ARL-TR-2696; U.S. Army Research Laboratory: Adelphi, MD, 2003.
4. Noble, J. M.; Marlin D. *User's Manual for the Scanning Fast Field Program (SCAFFIP) General Version 1.0*; ARL-TR-545; U.S. Army Research Laboratory: Adelphi, MD, 1995.
5. Albertson, J. D.; Katul, G. G.; Wiberg, P. Relative Importance of Local and Regional Controls on Coupled Water, Carbon, and Energy Fluxes. *Advances in Water Resources* **2001**, *24*, 1103–1118.
6. Srour, N. *Army Acoustics Needs: Sensor Arrays, Distributed Sensors and Applications*. DARPA Air-Coupled Acoustic Micro Sensors Workshop, Crystal City, VA, 24–25 August 1999.
7. Wilson, D. K. *A Prototype Acoustic Battlefield Decision Aid Incorporating Atmospheric Effects and Arbitrary Sensor Layouts*; ARL-TR-1708; U.S. Army Research Laboratory: Adelphi, MD, 1998.
8. Shinn, J. H. *Steady-State Two-Dimensional Air Flow in Forests and the Disturbance of Surface Layer Flow by a Forest Wall*; ECOM-5383; U.S. Army Electronics Command: Fort Monmouth, NJ, 1971.
9. Holland, J. Z. On Pressure-Driven Wind in Deep Forests. *Journal of Applied Meteorology* **1989**, *28*, 1349–1355.
10. Wilson, J. D.; Flesch, T. K. Wind and Remnant Tree Sway in Forest Cutblocks. III. A Windflow Model to Diagnose Spatial Variation. *Agricultural and Forest Meteorology* **1999**, *93*, 259–282.
11. Katul, G. G.; Albertson, J. D. An Investigation of Higher-Order Closure Models for a Forested Canopy. *Boundary-Layer Meteorology* **1998**, *89*, 47–74.
12. Meyers, T. P.; Paw U, K. T. Modeling the Plant Canopy Micrometeorology With Higher Order Closure Principles. *Agricultural and Forest Meteorology* **1987**, *41*, 143–163.

13. Wilson, N. R.; Shaw, R. H. A Higher Order Model for Canopy Flow. *Journal of Applied Meteorology* **1977**, *16*, 1197–1205.
14. Mellor, G. L. Analytic Prediction of the Properties of Stratified Planetary Surface Layers. *Journal of Atmospheric Science* **1973**, *30*, 1061–1069.
15. Mellor, G. L.; Yamada, T. A Hierarchy of Turbulence Closure Models for Planetary Boundary Layer. *Journal of Atmospheric Science* **1974**, *31*, 1791–1806.
16. Mellor, G. L.; Yamada, T. Development of a Turbulence Closure Model for Geophysical Fluid Problems. *Review of Geophysical and Space Physics* **1982**, *20*, 851–875.
17. Donaldson, C. Du P. Construction of a Dynamic Model for the Production of Atmospheric Turbulence and the Dispersion of Atmospheric Pollutants. In *Workshop on Micrometeorology*, American Meteorological Society, 1973; pp 313–392.
18. Rachele, H.; Tunick, A. Energy Balance Model for Imagery and Electromagnetic Propagation, *Journal of Applied Meteorology* **1984**, *33*, 964–976.
19. Weiss, A.; Norman, J. M. Partitioning Solar-Radiation into Direct and Diffuse, Visible and Near-Infrared Components. *Agricultural and Forest Meteorology* **1985**, *34*, 205–213.
20. Campbell, G. S. *An Introduction to Environmental Biophysics*. Springer-Verlag: New York, 1977.
21. Campbell, G. S.; Norman, J. M. *An Introduction to Environmental Biophysics*, 2nd ed.; Springer-Verlag: New York, 1998.
22. Wilson, J. D. A Second-Order Closure Model for Flow Through Vegetation. *Boundary-Layer Meteorology* **1988**, *42*, 371–392.
23. Ferziger, J. H.; Perić, M. *Computational Methods for Fluid Dynamics*, 3rd ed.; Springer: Berlin, 2002.
24. Press, W. H.; Teukolsky, S. A.; Vetterling, W. T.; Flannery, B. P. *Numerical Recipes in Fortran*, 2nd ed.; Cambridge University Press: New York, 1992.
25. Mahrer, Y.; Pielke, R. A. The Effects of Topography on Sea and Land Breezes in a Two-Dimensional Numerical Model. *Monthly Weather Review* **1977**, *105*, 1151–1162.
26. Massman, W. J. Foliage Distribution in Old-Growth Coniferous Tree Canopies. *Canadian Journal of Forest Research* **1982**, *12*, 10–17.
27. Meyers, T. P.; Finkelstein, P.; Clarke, J.; Ellestad, T. G.; Sims, P. F. A Multilayer Model for Inferring Dry Deposition Using Standard Meteorological Measurements. *Journal of Geophysical Research* **1998**, *103*, 22645–22661.
28. Munn, R. E. *Descriptive Micrometeorology*. Academic Press: New York, 1966.
29. Kaimal, J. C.; Finnigan, J. J. *Atmospheric Boundary Layer Flows: Their Structure and Measurement*. Oxford University Press: New York, 1994.
30. Li, Z.; Lin, J. D.; Miller, D. R. Air Flow Over and Through a Forest Edge: A Steady-State Numerical Simulation *Boundary-Layer Meteorology* **1990**, *51*, 179–197.

31. Finnigan, J. J.; Brunet, Y. Turbulent Air Flow in Forests on Flat and Hilly Terrain. In *Wind and Trees*, edited by M. P. Coutts and J. Grace, Cambridge University Press: England, UK, 1995; pp 3–39.

INTENTIONALLY LEFT BLANK.